Geol. Mag. **153** (*4*), *2016, pp. 618–634.* © *Cambridge University Press 2015*
doi:10.1017/S0016756815000758

Mineralogical composition of and trace-element accumulation in lower Toarcian anoxic sediments: a case study from the Bilong Co. oil shale, eastern Tethys

XIUGEN FU*‡†, JIAN WANG*‡, XINGLEI FENG*, WENBIN CHEN*, DONG WANG*, CHUNYAN SONG*‡ & SHENGQIANG ZENG*

*Chengdu Institute of Geology and Mineral Resources, Chengdu 610081, China
‡Key Laboratory for Sedimentary Basin and Oil and Gas Resources, Ministry of Land and Resources, Chengdu 610081, China

(*Received* 30 November 2014; *accepted* 9 September 2015; *first published online* 4 November 2015)

Abstract – The sediments of organic-rich oil shales in the Bilong Co. area can be correlated with those of the early Toarcian anoxic black-shale events in Europe. The Bilong Co. sediments are rich in trace elements Se, Mo, Cd, As and Ni, and, to a lesser extent, Li, F, V, Co, Cu, Cs, Hg and Bi, in comparison to the upper continental crust. Thirty-two oil shale samples were collected from the Bilong Co. oil shale to evaluate the controlling factors of trace-element enrichment in the lower Toarcian anoxic sediments. Minerals identified in the Bilong Co. oil shale include calcite, quartz, illite, feldspar and dolomite, and trace amounts of siderite, magnesite, halite, haematite, zeolite, amphibole, gypsum, anhydrite, apatite, pyrite, sphalerite, barite and mixed-layer illite/smectite. Mineralogical and geochemical data show that seawater and hydrothermal activities are the dominant influences on the mineralogical composition and elevated trace-element concentrations in the oil shale. The clay minerals, quartz and feldspar in the Bilong Co. oil shale were derived from the Nadi Kangri volcanic rocks. Input of sediment from this source may have led to enrichment of trace elements Li, Cr and Cs in the oil shale. Carbonate minerals and nodular- and framboidal-pyrite are authigenic phases formed from seawater. The enrichment of V, Co, Ni, Cu, Mo, As, Se, Bi and U in the oil shale was owing to marine influence. Barite, sphalerite and fracture-filling pyrites were derived from hydrothermal solutions. High concentrations of F, Zn and Cd were probably derived from hydrothermal fluids.

Keywords. minerals in oil shale, trace elements in oil shale, marine influence, hydrothermal activity, Bilong Co. of Eastern Tethys.

1. Introduction

The enrichment of trace elements in organic-rich sediments has received much attention (e.g. Algeo & Maynard, 2004; Wei *et al*. 2012; Dai *et al*. 2013; Fu *et al*. 2013). Studies of the concentrations of redox-sensitive trace elements in marine sediments and sedimentary rocks can be used to infer palaeoredox conditions (Algeo & Maynard, 2004; Tribovillard *et al*. 2006; Pattan & Pearce, 2009; Hetzel *et al*. 2011; Westermann *et al*. 2013; Fu *et al*. 2014). The geochemical anomalies in coal and oil shale may also give rise to some health problems during their exploration and utilization (Bencko & Symon, 1977; Finkelman, Belkin & Zheng, 1999; Dai *et al*. 2008, 2012; Zhao *et al*. 2008). Anomalous trace elements in coal are usually related to volcanic ashes, groundwater, magmatic/hydrothermal fluids and detrital source rocks (e.g. Baruah *et al*. 2005; Dai *et al*. 2005, 2008, 2013; Seredin & Finkelman, 2008; Seredin & Dai, 2012; Zhao *et al*. 2012). Strong enrichments of redox-sensitive elements in organic-rich shales are possibly related to anoxic bottom waters (Algeo & Maynard, 2004; Hetzel *et al*. 2011). However, the mechanisms that control the enrichment of trace elements in anoxic sediments are still uncertain or incompletely understood.

The Bilong Co. oil shale is located in the southern part of the Qiangtang Basin (Fig. 1a), and the proved oil shale reserves are estimated to be 90.6 million tonnes (Liu *et al*. 2009). This oil shale zone, together with the Shengli River – Changshe Mountain oil shale zone found in the North Qiangtang Depression (Fu *et al*. 2009), represents a large marine oil shale resource in China. The Bilong Co. oil shale has been subjected to many geological studies owing to its economic significance (Wang & Zhang, 1987; Fu *et al*. 2011, 2012) and potential as a hydrocarbon source rock (Fu *et al*. 2008). Previous studies have described the content and vertical distribution of trace elements in the Bilong Co. oil shale (Fu *et al*. 2011). However, a detailed study of the mechanisms controlling the enrichment of trace elements in the oil shale of this area is not available in the literature.

The Bilong Co. oil shale is enriched in Li, F, V, Co, Ni, Cu, As, Se, Mo, Cd, Cs, Hg and Bi

†Author for correspondence: fuxiugen@126.com

https://doi.org/10.1017/S0016756815000758 Published online by Cambridge University Press

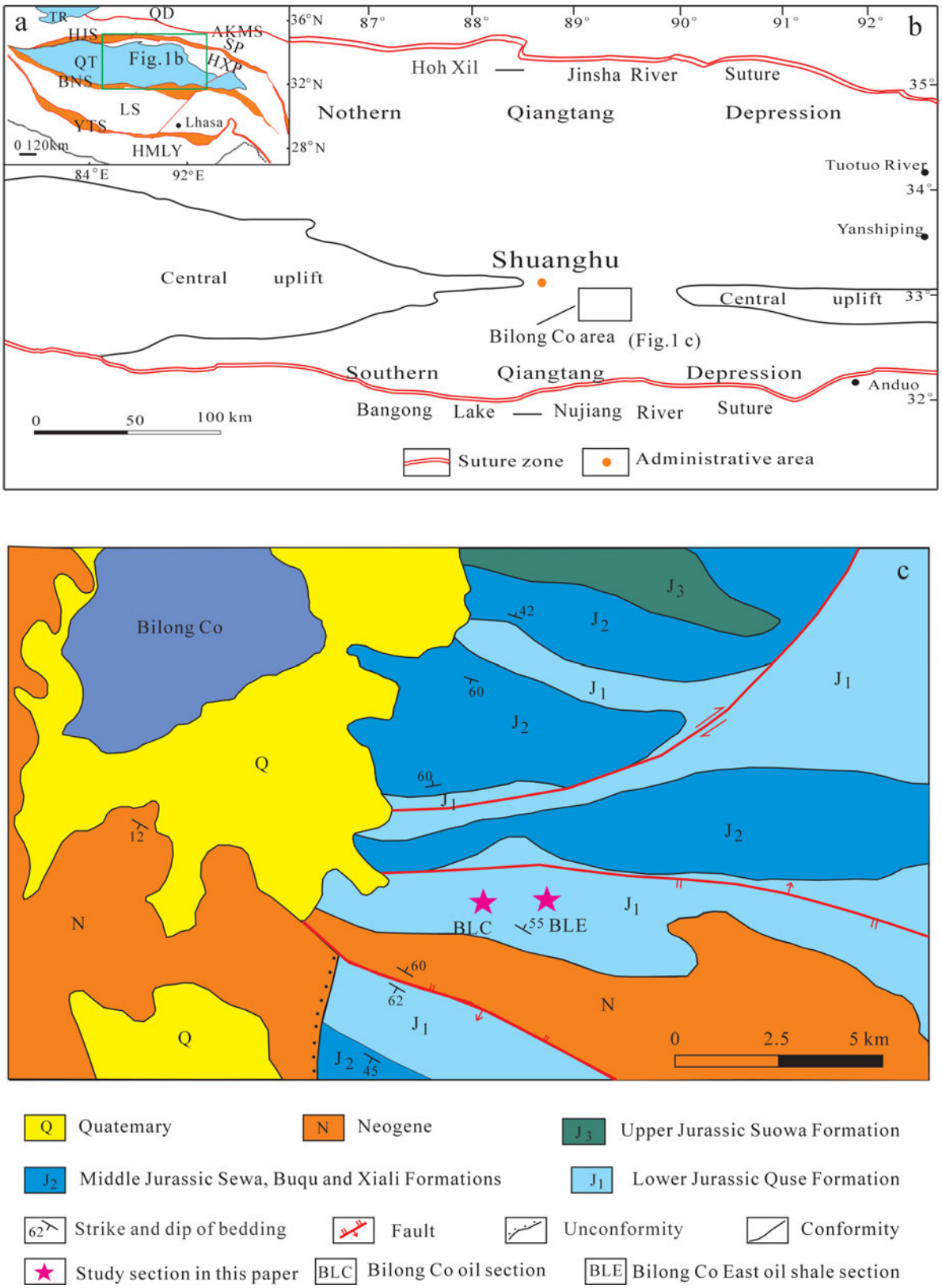

Figure 1. (Colour online) (a) Map of the Tibetan plateau showing major terranes (modified from Fu *et al*. 2010). (b) Generalized map, showing location of study area (modified from Fu *et al*. 2010). (c) Simplified geological map of the Bilong Co. area, showing location of the oil shale section (modified from Fu *et al*. 2011). TR – Tarim Basin; KLQD – Kunlun–Qaidam terrane; AKMS – Anyimaqen–Kunlun–Muztagh suture; HJS – Hoh Xil – Jinsha River suture; SP – Songpan–Ganzi flysch complex; HXP – Hoh Xili piedmont zone; QT – Qiagtang terrane; BNS – Bangong Lake – Nujiang River suture; LS – Lhasa terrane; YTS – Yarlung Tsangpo suture; HMLY – Himalayas.

https://doi.org/10.1017/S0016756815000758 Published online by Cambridge University Press

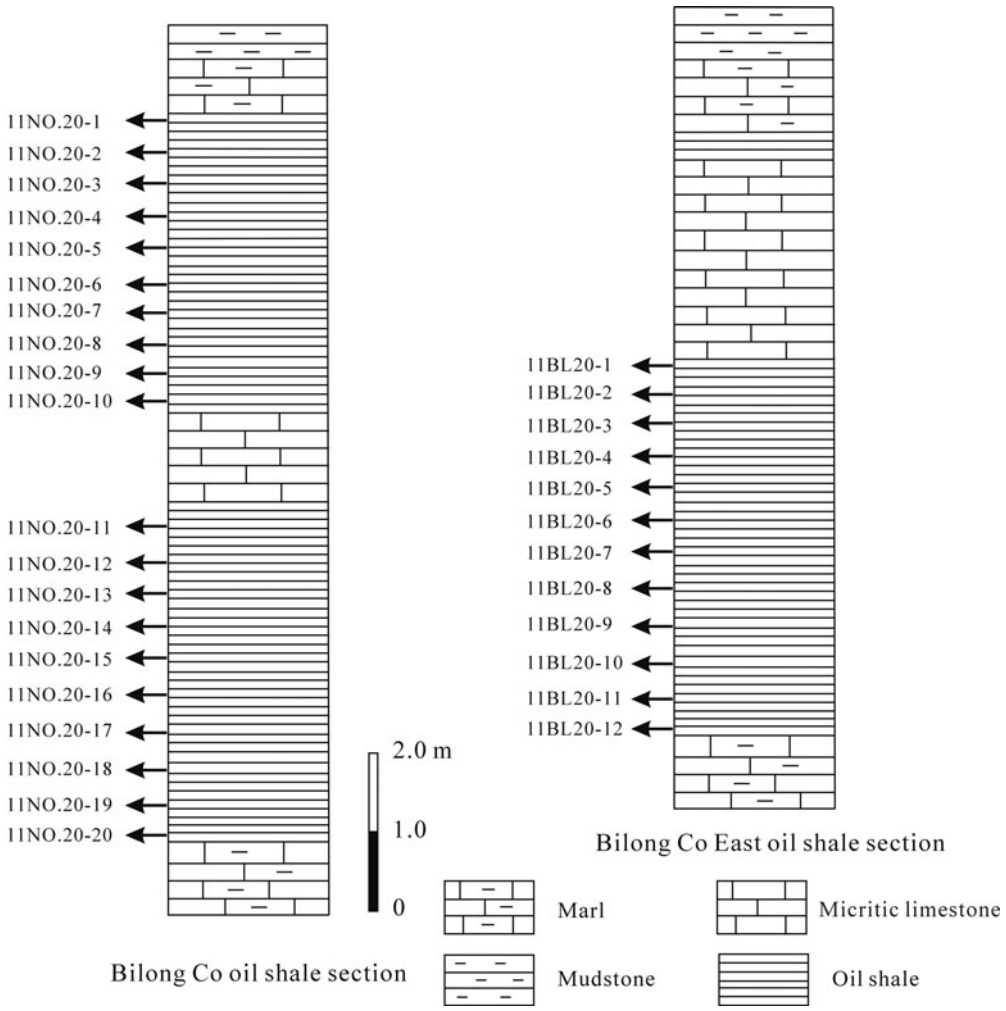

Figure 2. Sampling sections in the Bilong Co. oil shale showing sampling locations.

(see Section 4.d below). The organic-rich sediments in the Bilong Co. oil shale can be correlated with those of the early Toarcian anoxic black-shale events in Europe (Chen *et al*. 2005; Yi *et al*. 2013; Fu *et al*. 2014). Thus, the Bilong Co. oil shale provides a valuable reference for understanding the mechanisms of trace-element accumulation in the lower Toarcian anoxic sediments and in marine oil shale generally. The present study describes a detailed investigation of the concentrations of trace elements and minerals in the marine oil shale of the Bilong Co. area. The aims are to assess which factors controlled the enrichment of trace elements in the lower Toarcian anoxic sediments, and also in marine oil shale more generally.

2. Geological setting

The Qiangtang Terrane is one of three main E–W-trending continental terranes (i.e. Kunlun–Qaidam Terrane, Qiangtang Terrane and Lhasa Terrane) in the Qinghai–Tibet Plateau (Fig. 1a). It is bounded by the Hoh Xil – Jinsha River Suture Zone to the north and the Bangong Lake – Nujiang River Suture Zone to the south, respectively (Fig. 1b). The Qiangtang Terrane consists of the South Qiangtang Depression, the central uplift and the North Qiangtang Depression (Fig. 1b), which together form the Qiangtang Basin. The Qiangtang Basin is a residual Mesozoic marine sedimentary basin in which Jurassic sediments are the most widely distributed marine strata (Otto, 1997; Ding *et al*. 2011); Palaeozoic marine sedimentary sequences are locally preserved in the central uplift (Fu *et al*. 2013).

The Bilong Co. oil shale is located in the northern part of the South Qiangtang Depression, where the Jurassic marine deposits are most complete and extensive (Wang *et al*. 2004). These include the Lower Jurassic Quse Formation, Middle Jurassic Sewa, Buqu and Xiali formations, and Upper Jurassic Suowa Formation (Fu *et al*. 2011). The Bilong Co. oil shale was formed in Early Jurassic time (i.e. Quse Formation strata) (Fu *et al*. 2011). The sedimentary rocks in this unit are mainly made up of shale, marl, micritic limestone, mudstone and oil shale.

3. Materials and methods

The study area and section location are presented in Figure 1c. Thirty-two oil shale samples were taken from two sampling sections (Fig. 1c). Oil shale samples

https://doi.org/10.1017/S0016756815000758 Published online by Cambridge University Press

Table 1. Concentrations of TOC and major-element oxides and CIA values in oil shale samples from the Bilong Co. oil shale (units in %)

Sample nos.	lithology	TOC	M_{ad}	A_d	S_t	SiO_2	Al_2O_3	Fe_2O_3	FeO	CaO	MgO	K_2O	Na_2O	TiO_2	P_2O_5	MnO	CIA
11NO.20-1	oil shale	7.57	0.55	82.02	0.44	25.9	9.99	4.26	1.21	24.0	0.71	1.52	0.32	0.35	0.21	0.047	79
11NO.20-2	oil shale	8.66	0.53	84.92	0.40	28.1	10.1	3.86	1.59	21.3	0.74	1.78	0.32	0.39	0.24	0.044	77
11NO.20-3	oil shale	7.69	0.35	84.88	0.42	27.2	10.1	3.46	1.95	21.8	0.76	1.66	0.34	0.38	0.30	0.050	78
11NO.20-4	oil shale	11.0	0.41	67.08	0.40	19.2	6.90	2.68	0.97	31.6	0.74	1.14	0.28	0.26	0.29	0.037	76
11NO.20-5	oil shale	10.6	0.42	67.00	0.48	25.7	8.99	3.30	1.50	23.7	0.84	1.48	0.35	0.35	0.31	0.040	77
11NO.20-6	oil shale	9.21	0.95	64.98	0.44	19.1	7.04	3.34	1.21	29.5	0.84	1.14	0.27	0.26	0.21	0.040	77
11NO.20-7	oil shale	10.2	0.76	64.54	0.69	21.7	7.61	1.26	2.47	28.1	0.73	1.15	0.36	0.32	0.23	0.030	76
11NO.20-8	oil shale	8.63	0.72	68.39	0.36	22.0	8.10	1.78	2.18	28.2	0.75	1.41	0.39	0.30	0.29	0.042	74
11NO.20-9	oil shale	10.5	0.47	64.84	0.54	22.8	8.70	1.62	2.02	27.0	0.78	1.31	0.51	0.31	0.18	0.039	74
11NO.20-10	oil shale	10.2	0.80	62.91	0.72	21.9	7.72	1.97	1.70	28.0	0.74	1.30	0.34	0.32	0.21	0.034	75
11NO.20-11	oil shale	6.66	0.47	65.51	0.38	22.7	8.68	1.47	2.83	25.9	0.74	1.36	0.61	0.31	0.30	0.042	71
11NO.20-12	oil shale	8.49	0.46	62.65	0.92	20.3	7.69	1.91	1.97	28.5	0.69	1.16	0.34	0.29	0.25	0.032	76
11NO.20-13	oil shale	9.72	0.56	68.00	0.42	23.4	8.16	1.27	2.02	29.0	0.89	1.39	0.36	0.34	0.17	0.036	75
11NO.20-14	oil shale	6.09	0.50	64.27	0.22	19.1	6.72	1.30	1.89	33.1	0.82	1.12	0.30	0.26	0.13	0.034	75
11NO.20-15	oil shale	12.4	0.64	66.58	0.52	26.0	8.94	1.97	1.80	25.6	0.90	1.52	0.37	0.36	0.14	0.037	76
11NO.20-16	oil shale	10.5	0.36	66.39	0.34	25.4	8.88	2.13	1.58	26.3	0.85	1.47	0.35	0.35	0.15	0.038	76
11NO.20-17	oil shale	6.92	0.30	67.36	0.23	23.8	8.15	0.66	2.56	28.3	0.82	1.39	0.35	0.33	0.13	0.031	75
11NO.20-18	oil shale	6.12	0.44	79.36	0.26	22.2	7.73	1.90	1.92	28.1	0.83	1.24	0.33	0.30	0.18	0.042	76
11NO.20-19	oil shale	5.17	0.20	83.69	0.13	19.5	6.45	1.98	1.16	33.3	0.85	1.12	0.34	0.26	0.13	0.035	73
11NO.20-20	oil shale	15.2	0.85	85.20	0.66	22.0	7.91	3.11	1.70	26.4	0.81	1.25	0.36	0.31	0.26	0.050	76
11BL20-1	oil shale	3.73	0.15	90.49	0.15	22.9	7.62	2.04	1.16	30.0	0.82	1.29	0.34	0.31	0.12	0.032	75
11BL20-2	oil shale	9.27	0.90	65.34	0.24	16.5	5.72	1.72	1.30	35.1	0.91	0.94	0.24	0.22	0.18	0.040	76
11BL20-3	oil shale	6.14	0.62	67.37	0.34	22.3	8.43	2.35	1.72	27.6	0.83	1.35	0.31	0.30	0.19	0.052	77
11BL20-4	oil shale	7.69	0.30	66.52	0.49	22.9	8.96	2.70	2.02	26.5	0.80	1.35	0.38	0.32	0.20	0.058	77
11BL20-5	oil shale	6.19	1.10	72.45	0.62	21.8	8.88	2.77	1.92	26.5	0.78	1.24	0.38	0.30	0.23	0.050	77
11BL20-6	oil shale	6.79	0.20	62.47	0.58	20.6	7.68	1.72	2.09	28.6	0.80	1.20	0.32	0.28	0.20	0.046	77
11BL20-7	oil shale	6.08	0.56	64.58	0.56	20.8	8.09	2.36	1.48	28.4	0.75	1.22	0.32	0.28	0.20	0.044	77
11BL20-8	oil shale	6.58	0.50	66.76	0.54	22.9	9.14	1.91	1.98	26.5	0.75	1.31	0.34	0.30	0.18	0.043	78
11BL20-9	oil shale	5.29	1.00	66.77	1.78	25.0	8.92	3.09	1.60	28.4	0.79	1.51	0.36	0.34	0.17	0.038	76
11BL20-10	oil shale	6.59	1.50	67.53	2.26	21.1	7.38	2.68	1.52	31.3	0.76	1.25	0.32	0.29	0.19	0.040	75
11BL20-11	oil shale	4.62	0.68	72.44	0.46	25.3	8.79	2.97	1.47	25.7	0.81	1.55	0.31	0.35	0.26	0.048	76
11BL20-12	oil shale	7.33	0.30	67.20	1.94	25.0	8.83	3.53	1.38	24.3	0.82	1.53	0.30	0.35	0.33	0.042	77

TOC – total organic carbon; M – moisture; A – ash yield; S_t – total sulfur; ad – air-dry basis; d – dry basis; CIA – chemical index of alteration.

11NO.20 were sampled from the Bilong Co. oil shale section, while oil shale samples 11BL20 were taken from the Bilong Co. East oil shale section (Fig. 2). In the Bilong Co. oil shale section, ten oil shale samples (11NO.20-1–11NO.20-10) were taken from the *c*. 4.0 m thick upper oil shale bed with a uniform sampling interval of *c*. 40 cm (Fig. 2). The other ten samples (11NO.20-11–11NO.20-20) in the Bilong Co. oil shale section were taken from a *c*. 5.0 m thick lower oil shale bed with a uniform sampling interval of *c*. 50 cm. In the Bilong Co. East oil shale section, 12 oil shale samples were collected from a *c*. 5.5 m thick oil shale bed with a uniform sampling interval of *c*. 50 cm (Fig. 2). Samples from these areas were collected from surface exposures. All collected samples were immediately stored in plastic bags to minimize contamination.

Total organic carbon (TOC) was determined using a LECO CS-200 carbon-sulfur analyser with crushed samples (120 mesh) heated from ambient temperature to 1200 °C in an induction furnace after removing carbonate by hydrochloric acid. Analytical procedures are described more fully by Yeomans & Bremner (1988).

A scanning electron microscope (SEM) (Hitachi S-3400N), in conjunction with an energy-dispersive X-ray spectrometer (SEM-EDX), was used to study the morphology of the minerals, and also to determine the distribution of some elements in the oil shale samples, using a 20-kV accelerating voltage and a 10^{-10} – A beam current. The SEM images were taken from polished sections (polished blocks rather than grain mounts) of the oil shale samples.

The mineralogy was determined by optical microscopic observation and by X-ray powder diffraction (XRD). XRD analysis was performed on a D8 ADVANCE powder diffractometer equipped with a Cu-target tube and a curved graphite monochromator. The XRD pattern was recorded over an interval of 2θ (3°–70°), with a step size of 0.01°. The analytical procedures were taken from Chinese National Standard SY/T 6210-1996 (1996). XRD results were subjected to quantitative mineralogical analysis using Diffrace Plus Eva, an interpretation software developed by Bruker Instrument Co. Ltd based on the reference intensity ratio (RIR) approach (Hillier, 2000). The proportion of clay minerals was based on particular phases.

Samples were crushed and ground to less than 200 mesh (75 μm) for geochemical analysis. X-ray fluorescence spectrometry (XRF) was used to determine the oxides of major elements in the oil shale (850 °C), including SiO_2, Al_2O_3, CaO, K_2O, Na_2O, Fe_2O_3, MnO, MgO, TiO_2 and P_2O_5. FeO was determined by titration with potassium dichromate ($K_2Cr_2O_7$). Inductively coupled plasma mass spectrometry (ICP-MS) was used to determine trace elements in the oil shale samples, following the Chinese National Standard method DZ/T 0223-2001 (2001). The oil shale samples for ICP-MS

https://doi.org/10.1017/S0016756815000758 Published online by Cambridge University Press

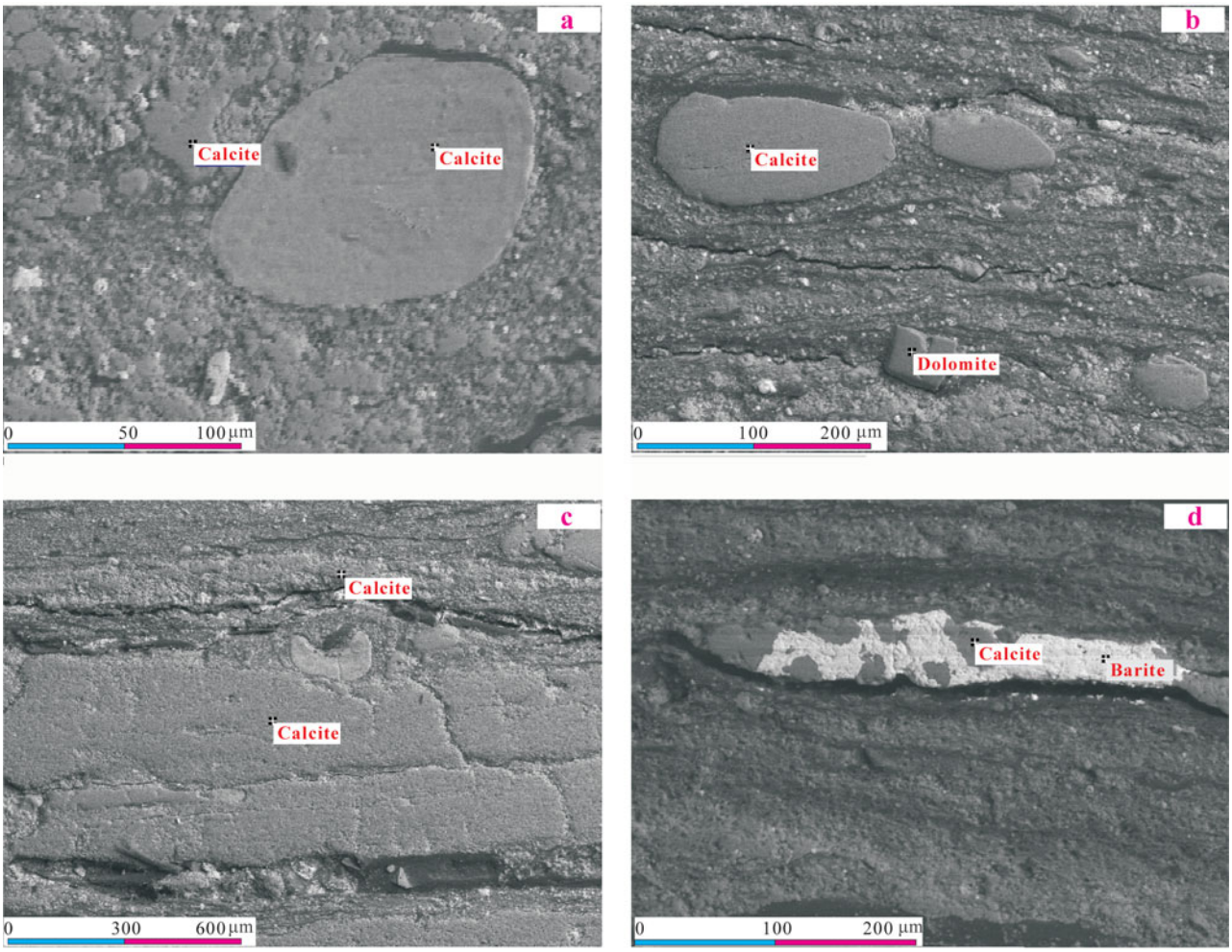

Figure 3. (Colour online) SEM and back-scattered electron image of carbonate minerals in the oil shale samples. (a) Disseminated-grain calcite, sample 11NO.20-2; (b) disseminated-grain calcite and dolomite, sample 11NO.20-3; (c) banded calcite, sample 11NO.20-3; and (d) fracture-filling calcite and barite, sample 11BL20-3.

Table 2. Mineral content as inferred from semi-quantitative XRD analysis in the Bilong Co. oil shale (units in %)

Sample nos.	Quartz	Feldspar	Calcite	Dolomite	Siderite	Magnesite	Halite	Haematite	Zeolite	Amphibole	Gypsum	Anhydrite	Clay minerals
11NO.20-2	14.0	2.4	56.6										27.0
11NO.20-3	25.7		67.3										7.00
11NO.20-4	13.7		73.4		1.9								11.0
11NO.20-5	12.5	2.3	57.0	2.0							0.3		25.9
11NO.20-6	5.4	1.4	87.1	1.1									5.00
11NO.20-12	13.1	3.4	78.0						1.2	1.3			3.00
11NO.20-13	11.5	5.7	67.3	8.5					2.0				5.00
11NO.20-15	11.8		56.8	1.4		0.8		1.0				3.0	25.2
11NO.20-16	12.6		80.4	1.0						1.0			5.0
11NO.20-18	12.1	4.0	59.6		1.0		0.3						23.0
11BL20-1	10.4	3.7	65.6										20.3
11BL20-3	11.5		67.4	2.5				0.4					18.2
11BL20-7	11.0	4.1	74.4								0.4		10.1

analysis were digested in a microwave furnace using $HF + HNO_3$ ($HF:HNO_3 = 1:2$). Arsenic, Se and Hg were determined by atomic fluorescence spectrometry, using the Chinese Standard method DZG 20.10-1990 (1990).

4. Results

4.a. TOC values

The TOC contents of 32 oil shale samples from the Bilong Co. area range from 3.73 to 15.2 % (Table 1). The

https://doi.org/10.1017/S0016756815000758 Published online by Cambridge University Press

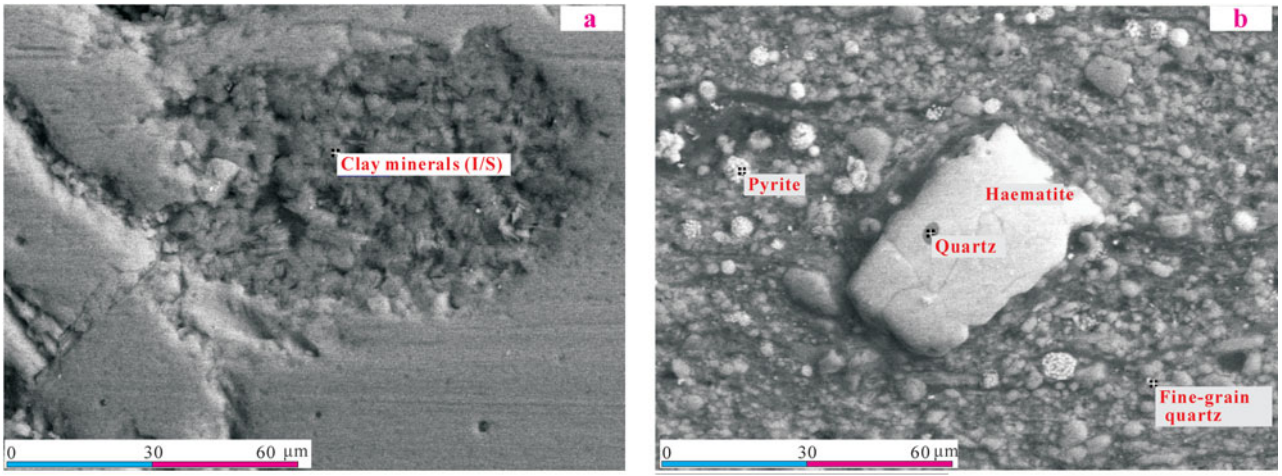

Figure 4. (Colour online) Modes of occurrence of clay and quartz in the oil shale samples. (a) Irregular-filling mixed-layer (I/S) clay minerals with a colloform texture, sample 11NO.20-9; (b) fine-grained quartz restricted to the haematite and fine-grained quartz forming a matrix, sample 11NO.20-6 (SEM and back-scattered electron image).

Bilong Co. oil shale section shows slightly higher concentrations of organic matter (5.17–15.2 %) compared with the Bilong Co. East oil shale section (3.73–9.27 %) (Table 1).

4.b. Minerals

The minerals identified from the XRD data in the whole-oil shale samples are abundant calcite, quartz and illite, minor quantities of feldspar, dolomite and mixed-layer illite/smectite (I/S) (Fig. 4a), and trace amounts of siderite, magnesite, halite, haematite, zeolite, amphibole, gypsum and anhydrite (Table 2). Apatite, pyrite, sphalerite and barite were also identified in some oil shale samples by SEM-EDX, but were below the detection limit of the XRD.

Carbonate minerals are the most common phase including calcite, dolomite, siderite and magnesite. They mainly occur as disseminated grains (Figs 3a, b) and banded (Fig. 3c), and partly as fracture-fillings (Fig. 3d). Microscopic observation suggests that the calcite bands represent algal bodies in the oil shale. Clay minerals were identified in the oil shale samples. They generally occur as irregular masses (Fig. 4a). Quartz occurs as fine particles forming a matrix (Fig. 4b) or as fine grains restricted to the haematite (Fig. 4b). Pyrite is the most common S-bearing mineral in the Bilong Co. oil shale. It was found mainly as nodular (Fig. 5a) and framboidal forms (Figs 4b, 5b), and partly as replacement forms (Figs 5c, d), indicating that the pyrite in the Bilong Co. oil shale is mainly of syngenetic or early diagenetic origin. Additionally, fracture-filling pyrite (Fig. 5e, f) was also found in some oil shale samples, indicating an epigenetic origin. Other S-bearing minerals, including sphalerite (Fig. 6), were found in several of the oil shale samples.

Apatite was identified in almost all oil shale samples by SEM analysis, and occurs mainly as fracture-fillings (Figs 7a, b). Other minerals including haematite (Fig. 4b) and barite (Fig. 8), were also identified in some oil shale samples using SEM-EDX analysis.

4.c. Major-element geochemistry

The major oxides in oil shale samples from the Bilong Co. oil shale are CaO (21.3–35.1 %), SiO_2 (16.5–28.1 %) and Al_2O_3 (5.72–10.1 %). Fe_2O_3, FeO and K_2O are the second most abundant oxides, while all other oxides (MgO %, Na_2O %, TiO_2 %, P_2O_5 % and MnO %) have concentrations of < 1.0 % (Table 1).

The high CaO content probably reflects the abundant calcite and dolomite in the Bilong Co. oil shale samples, although Ca may also be partly present as zeolite, gypsum, anhydrite (Table 2) and apatite. Aluminium and Si also show high abundances in the Bilong Co. oil shale, which is consistent with the abundant clay minerals and quartz identified by XRD (Table 2) and SEM-EDX analyses (Fig. 4). Additionally, Si and Al may also be partly associated with zeolite and/or amphibole (Table 2). The high Fe_2O_3 and FeO contents probably reflect the Fe-bearing minerals, including pyrite (Fig. 5), haematite (Fig. 4b) and siderite (Table 2). A significant positive correlation between Al_2O_3 and TiO_2 ($r = 0.98$) and K_2O ($r = 0.97$) indicates that these elements have similar carriers. Mg is probably contained in the dolomite, the clay minerals and magnesite, and P is probably contained in apatite observed by SEM-EDX analyses.

4.d. Trace elements in the Bilong Co. oil shale

The concentrations of trace elements in the 32 samples from the Bilong Co. oil shale are presented in Table 3. Based on average values, the most abundant trace elements are F (average 823 μg/g), V (average 126 μg/g), Sr (average 396 μg/g) and Ba (average 285 μg/g).

Compared to the average concentration in the upper continental crust (UCC) reported by Taylor & McLennan (1995), trace elements Se, Mo, Cd, As and Ni are

https://doi.org/10.1017/S0016756815000758 Published online by Cambridge University Press

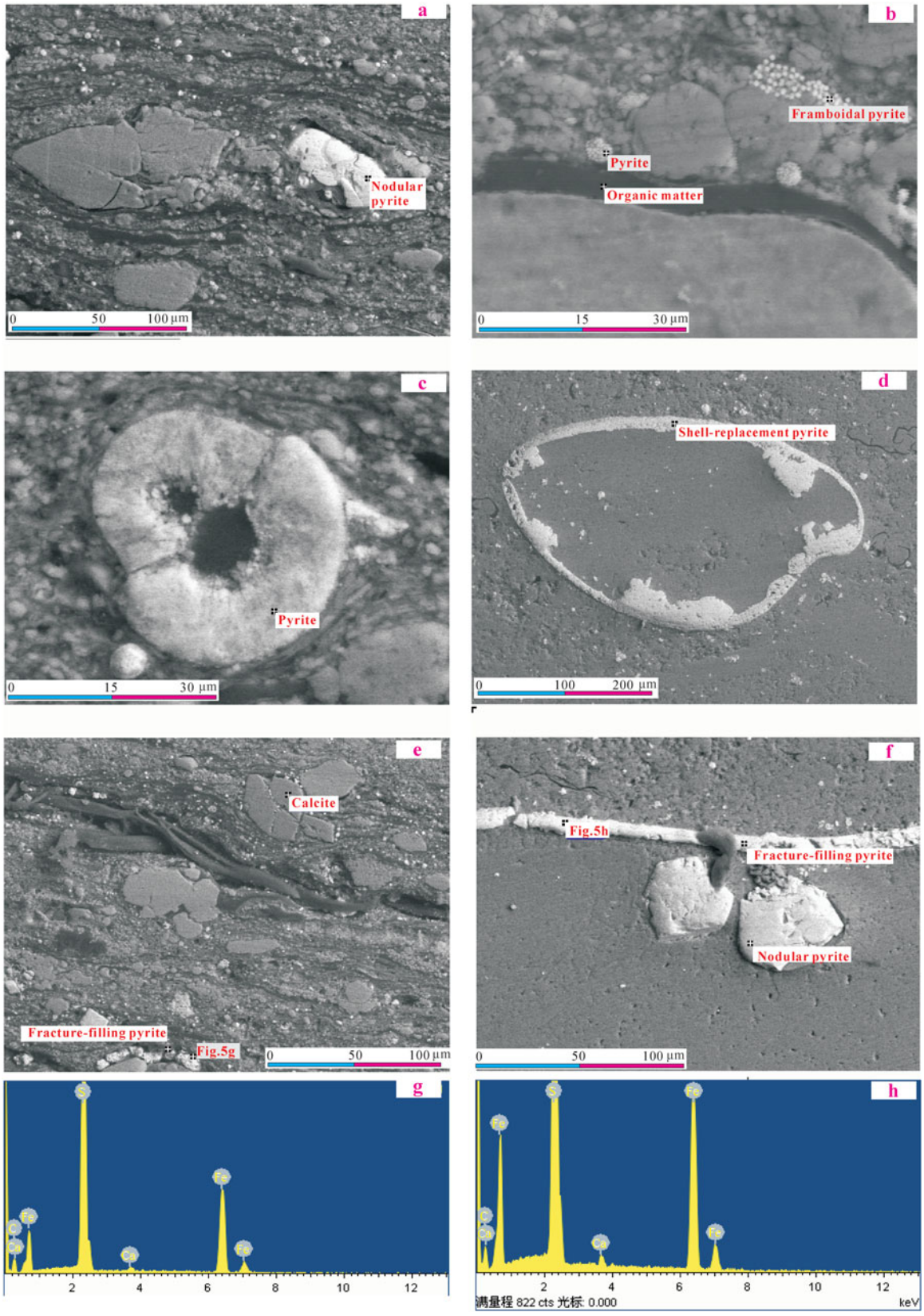

Figure 5. (Colour online) Pyrite identified by SEM (back-scattered images) and EDX spectra in the Bilong Co. oil shale. (a) Nodular pyrite, 11NO.20-4; (b) framboidal-pyrite and organic matter, sample 11NO.20-7; (c) replacement pyrite, sample 11NO.20-6; (d) shell-replacement pyrite, sample 11BL20-4; (e, f) fracture-filling pyrite, samples 11NO.20-15 and 11BL20-8; and (g, h) pyrite identified by EDX spectra in the oil shale samples.

https://doi.org/10.1017/S0016756815000758 Published online by Cambridge University Press

https://doi.org/10.1017/S0016756815000758 Published online by Cambridge University Press

Table 3. Concentrations of trace elements in samples from the Bilong Co. oil shale (units in μg/g)

Sample nos.	11 NO. 20-1	11 NO. 20-2	11 NO. 20-3	11 NO. 20-4	11 NO. 20-5	11 NO. 20-6	11 NO. 20-7	11 NO. 20-8	11 NO. 20-9	11 NO. 20-10	11 NO. 20-11	11 NO. 20-12	11 NO. 20-13	11 NO. 20-14	11 NO. 20-15	11 NO. 20-16	11 NO. 20-17	11 NO. 20-18
Li	38.1	39.8	39.2	26.1	35.0	27.4	28.9	30.5	31.8	30.6	32.3	29.6	31.0	25.2	36.5	34.0	32.4	31.4
Be	1.61	1.78	1.80	1.37	1.60	1.26	1.24	1.50	1.35	1.29	1.45	1.25	1.31	0.97	1.52	1.46	1.37	1.38
F	790	940	920	800	910	780	900	810	880	780	830	790	770	720	890	870	870	830
Sc	9.75	9.28	9.28	6.68	8.16	6.86	6.50	7.47	7.44	7.17	7.72	6.88	7.58	6.40	8.50	8.35	7.60	7.45
V	143	144	150	134	138	132	122	138	119	122	143	129	117	93.3	120	114	107	115
Cr	58.9	60.2	61.6	44.9	55.0	43.2	45.0	56.8	45.8	52.3	53.4	46.7	48.9	36.4	50.7	48.8	47.1	45.2
Co	21.2	20.3	23.1	13.6	19.2	17.6	14.7	15.7	16.9	13.8	17.7	15.2	13.9	12.4	19.1	18.4	14.5	17.3
Ni	91.2	93.2	109.0	69.9	100.0	92.2	90.8	84.1	77.3	85.4	93.7	99.3	66.3	58.2	79.5	72.8	71.0	77.3
Cu	71.8	70.9	75.5	46.7	69.7	71.4	44.8	52.7	48.3	40.9	64.5	48.1	39.4	33.3	53.4	50.4	39.7	53.5
Zn	113.0	59.6	103.0	46.9	41.5	328.0	71.4	65.1	83.6	77.3	96.2	112.0	35.0	51.0	75.5	61.3	132.0	276.0
Ga	12.10	12.10	11.90	8.00	10.40	8.18	8.64	8.97	9.24	8.65	9.63	8.32	9.45	7.19	10.90	10.60	9.62	9.29
As	13.40	12.10	13.00	9.31	9.64	10.30	7.99	10.90	8.71	7.89	10.80	8.70	6.64	6.19	11.60	8.75	7.43	10.30
Se	3.57	3.61	4.00	2.25	3.01	3.32	4.46	3.27	2.84	3.03	3.62	2.24	1.99	1.18	1.51	1.31	1.22	1.89
Rb	100.0	106.0	104.0	70.4	91.6	68.8	75.9	81.5	79.3	77.3	84.3	71.7	81.2	60.1	89.2	85.7	79.1	75.6
Sr	617	512	428	452	352	363	403	470	345	393	369	415	441	424	365	359	365	360
Y	14.1	13.9	14.6	10.2	13.1	11.0	10.3	11.2	11.4	10.5	12.1	10.4	11.7	9.91	12.4	12.3	10.8	11.4
Zr	67.1	72.0	71.5	50.2	68.5	49.5	57.6	56.7	58.9	58.6	59.2	53.0	61.9	47.6	70.7	67.7	59.0	62.4
Nb	8.23	8.97	8.73	6.06	7.85	5.84	6.88	6.86	7.04	6.94	7.22	6.41	7.48	5.65	8.16	7.87	7.18	6.85
Mo	22.8	26.2	40.2	24.6	36.8	43.1	52.0	27.8	51.3	48.1	37.8	63.8	31.3	42.4	52.9	49.7	49.5	53.5
Cd	1.37	0.74	1.25	0.61	0.54	3.77	1.23	1.32	1.22	1.25	1.09	2.00	0.48	0.66	0.83	0.80	0.91	2.51
Sn	2.72	2.66	2.64	1.90	2.49	1.89	1.94	2.27	2.15	1.97	2.17	1.90	2.20	1.78	2.16	2.26	2.15	2.03
Cs	8.78	9.12	9.15	6.06	7.91	5.81	6.30	6.91	6.65	6.38	7.18	6.06	6.60	5.03	7.31	7.26	6.47	6.51
Ba	285	306	310	412	518	219	450	296	237	325	270	290	245	194	350	346	311	220
La	20.0	20.6	20.7	14.3	18.7	15.2	16.0	16.4	17.0	16.3	17.3	15.2	17.9	14.9	19.2	19.3	16.4	16.9
Ce	39.5	41.0	41.6	28.2	37.8	29.4	31.5	32.0	33.6	31.7	34.2	29.9	34.9	29.3	37.7	38.3	32.1	33.6
Pr	4.48	4.71	4.72	3.29	4.27	3.34	3.61	3.67	3.97	3.66	4.01	3.47	4.13	3.41	4.35	4.49	3.77	3.86
Nd	17.2	17.5	17.4	12.1	15.5	12.6	13.2	13.4	14.5	13.5	14.6	12.9	15.0	13.0	16.3	16.5	13.8	14.1
Sm	3.36	3.44	3.62	2.45	3.06	2.70	2.67	2.79	2.82	2.57	2.97	2.66	2.89	2.62	3.09	3.31	2.76	2.93
Eu	0.71	0.71	0.76	0.52	0.69	0.56	0.51	0.58	0.58	0.53	0.60	0.55	0.60	0.53	0.70	0.66	0.57	0.63
Gd	3.20	3.19	3.41	2.30	3.11	2.39	2.48	2.38	2.60	2.31	2.82	2.25	2.78	2.31	2.81	3.17	2.39	2.66
Tb	0.47	0.47	0.48	0.33	0.43	0.35	0.36	0.38	0.38	0.34	0.41	0.33	0.40	0.35	0.42	0.43	0.34	0.39
Dy	2.71	2.85	2.90	1.97	2.61	2.12	2.03	2.15	2.20	2.04	2.43	1.94	2.32	1.98	2.37	2.45	2.09	2.20
Ho	0.53	0.57	0.59	0.40	0.52	0.42	0.40	0.42	0.44	0.41	0.46	0.39	0.47	0.38	0.47	0.48	0.39	0.44
Er	1.59	1.67	1.70	1.12	1.52	1.24	1.18	1.31	1.26	1.19	1.42	1.21	1.31	1.17	1.41	1.42	1.17	1.23
Tm	0.20	0.23	0.23	0.15	0.19	0.17	0.16	0.16	0.18	0.16	0.19	0.15	0.18	0.15	0.18	0.19	0.17	0.17
Yb	1.41	1.50	1.53	1.03	1.44	1.08	1.03	1.19	1.15	1.08	1.27	1.04	1.21	1.05	1.25	1.28	1.08	1.09
Lu	0.20	0.23	0.21	0.16	0.20	0.17	0.18	0.18	0.16	0.16	0.19	0.15	0.19	0.15	0.20	0.19	0.15	0.16
Hf	1.95	2.06	2.12	1.47	1.99	1.47	1.72	1.61	1.78	1.69	1.68	1.51	1.91	1.48	2.03	2.00	1.67	1.81
Ta	0.58	0.62	0.64	0.44	0.59	0.43	0.49	0.52	0.51	0.49	0.54	0.44	0.54	0.41	0.59	0.58	0.50	0.50
W	0.68	0.74	0.80	0.55	0.73	0.55	0.68	0.63	0.69	0.66	0.68	0.61	0.64	0.58	0.74	0.76	0.65	0.65
Hg	0.021	0.028	0.044	0.028	0.039	0.035	0.023	0.028	0.030	0.022	0.028	0.026	0.024	0.012	0.030	0.023	0.021	0.025
Pb	25.2	26.4	27.5	18.1	26.0	23.0	18.7	19.7	19.2	17.9	23.8	19.5	16.8	16.9	22.2	21.6	18.4	19.3
Bi	0.42	0.42	0.45	0.30	0.44	0.37	0.29	0.34	0.29	0.30	0.39	0.31	0.27	0.23	0.34	0.33	0.29	0.31
Th	6.92	7.53	7.64	5.19	7.07	5.23	5.51	5.84	6.08	5.61	6.27	5.41	6.24	5.01	6.84	6.88	5.86	5.94
U	3.52	3.76	4.50	3.27	4.86	4.88	4.17	3.48	4.08	4.05	4.28	4.43	3.49	3.40	4.51	4.33	3.71	4.25

https://doi.org/10.1017/S0016756815000758 Published online by Cambridge University Press

Table 3. (Continued)

Sample nos.	11 NO. 20-19	11 NO. 20-20	11 BL 20-1	11 BL 20-2	11 BL 20-3	11 BL 20-4	11 BL 20-5	11 BL 20-6	11 BL 20-7	11 BL 20-8	11 BL 20-9	11 BL 20-10	11 BL 20-11	11 BL 20-12	Av	UCC	EF
Li	25.4	35.9	30.4	22.6	34.2	35.6	34.1	30.5	29.6	32.1	32.4	28.5	34.6	36.1	31.93	20	1.60
Be	1.08	1.34	1.20	1.02	1.36	1.34	1.45	1.35	1.19	1.39	1.37	1.18	1.57	1.69	1.38	3	0.46
F	1200	850	700	620	790	840	790	800	820	870	490	690	890	900	823	540	1.52
Sc	6.55	7.76	7.54	5.79	8.48	8.17	7.64	7.08	7.11	7.60	7.65	6.96	8.53	8.36	7.63	11	0.69
V	96.1	142	97.4	108	139	142	140	124	114	116	129	121	145	148	126	60	2.11
Cr	41.7	49.1	43.4	37.4	50.1	53.6	47.0	44.8	43.5	44.8	50.5	47.8	53.4	55.3	48.9	35	1.40
Co	12.7	20.9	14.2	14.2	20.3	22.0	19.9	17.5	17.2	18.2	16.3	15.6	17.1	19.0	17.2	10	1.72
Ni	65.5	95.9	64.5	60.0	85.2	90.4	95.4	74.1	74.3	76.8	91.2	89.1	77.3	104.0	83.0	20	4.15
Cu	33.6	64.1	34.8	43.1	73.2	78.8	65.5	61.4	55.1	55.0	50.4	48.0	63.2	64.6	55.2	25	2.21
Zn	36.2	94.8	72.1	45.0	53.6	76.4	102.0	206.0	198.0	104.0	62.7	79.1	42.9	56.0	95.5	71	1.35
Ga	7.59	9.27	8.88	6.70	9.85	9.68	9.01	8.69	8.72	9.59	9.45	8.22	10.70	10.30	9.37	17	0.55
As	6.33	12.5	7.42	8.14	10.90	13.00	11.90	9.95	9.11	8.63	8.69	8.54	11.20	13.30	9.79	1.5	6.53
Se	1.21	2.61	2.66	1.21	1.45	1.77	2.50	1.96	1.81	1.80	1.82	3.09	2.84	2.41	2.42	0.05	48.41
Rb	63.3	78.7	73.2	55.1	82.5	81.8	78.5	74.1	72.3	79.0	81.6	69.2	89.2	91.0	79.7	112	0.71
Sr	425	428	382	426	373	361	424	349	346	322	318	333	372	382	396	350	1.13
Y	9.71	14.0	12.7	9.53	18.0	13.4	12.4	11.6	11.3	11.6	13.8	13.0	14.2	12.8	12.2	22	0.55
Zr	51.4	57.8	66.2	40.5	58.2	60.6	57.8	51.9	53.5	58.5	61.2	53.3	66.9	63.2	59.2	190	0.31
Nb	5.96	6.86	6.72	5.53	6.94	7.11	6.88	6.29	6.28	7.00	7.21	6.20	7.91	7.82	7.03	25	0.28
Mo	42.9	70.0	46.5	33.4	45.7	50.7	57.3	47.1	56.5	57.2	48.1	46.3	38.1	44.8	45.0	1.5	29.97
Cd	0.52	1.61	0.64	0.54	0.76	1.26	1.77	2.17	2.79	1.30	1.25	2.36	0.98	0.66	1.29	0.098	13.13
Sn	1.87	2.07	2.01	1.65	2.11	2.01	2.05	1.94	1.94	2.18	2.07	1.95	2.35	2.31	2.12	5.5	0.39
Cs	5.27	6.86	5.95	4.60	6.87	7.07	6.70	6.15	6.04	6.51	6.51	5.83	7.41	7.77	6.72	3.7	1.82
Ba	227	203	367	283	367	238	209	244	235	215	197	160	259	340	285	550	0.52
La	14.5	18.3	16.6	13.0	19.1	18.7	17.6	16.2	16.4	17.2	18.4	17.3	20.1	18.6	17.3	30	0.58
Ce	28.2	35.5	31.8	25.1	36.0	37.2	35.0	31.7	32.5	34.0	35.7	33.4	39.3	37.2	34.0	64	0.53
Pr	3.26	4.32	3.73	2.92	4.43	4.37	4.10	3.71	3.77	3.96	4.13	3.89	4.58	4.20	3.96	7.1	0.56
Nd	12.3	15.9	13.9	10.9	16.5	16.5	15.3	13.5	13.9	14.5	15.0	14.4	17.1	15.5	14.6	26	0.56
Sm	2.42	3.38	2.95	2.19	3.50	3.27	3.16	2.79	2.84	3.02	3.25	2.94	3.44	3.25	2.97	4.5	0.66
Eu	0.51	0.74	0.54	0.48	0.74	0.71	0.67	0.57	0.60	0.64	0.67	0.64	0.71	0.63	0.62	0.88	0.70
Gd	2.13	3.17	2.63	2.09	3.52	3.45	2.84	2.59	2.67	2.69	3.08	2.81	3.20	3.07	2.77	3.8	0.73
Tb	0.31	0.47	0.38	0.29	0.56	0.46	0.43	0.38	0.38	0.40	0.44	0.41	0.46	0.41	0.40	0.64	0.63
Dy	1.85	2.75	2.24	1.72	3.34	2.68	2.50	2.30	2.30	2.33	2.65	2.38	2.68	2.57	2.36	3.5	0.68
Ho	0.37	0.50	0.46	0.35	0.67	0.50	0.48	0.42	0.45	0.45	0.54	0.48	0.54	0.51	0.47	0.8	0.58
Er	1.04	1.53	1.35	0.97	2.04	1.54	1.39	1.32	1.28	1.23	1.61	1.42	1.55	1.46	1.37	2.3	0.60
Tm	0.15	0.20	0.19	0.13	0.29	0.20	0.20	0.15	0.16	0.17	0.21	0.19	0.21	0.19	0.18	0.33	0.55
Yb	0.98	1.34	1.34	0.91	1.74	1.34	1.27	1.13	1.15	1.19	1.42	1.22	1.39	1.39	1.24	2.2	0.56
Lu	0.14	0.21	0.18	0.14	0.26	0.19	0.18	0.17	0.17	0.17	0.23	0.19	0.20	0.21	0.18	0.32	0.57
Hf	1.50	1.53	1.90	1.15	1.68	1.77	1.63	1.55	1.62	1.70	1.80	1.55	1.95	1.83	1.72	5.8	0.30
Ta	0.44	0.49	0.49	0.36	0.51	0.52	0.48	0.45	0.48	0.50	0.53	0.45	0.59	0.56	0.51	2.2	0.23
W	0.53	0.68	0.62	0.46	0.65	0.58	0.58	0.61	0.62	0.68	0.60	0.50	0.65	0.71	0.64	2.0	0.32
Hg	0.042	0.028	0.024	0.026	0.028	0.031	0.022	0.029	0.019	0.024	0.031	0.021	0.031	0.037	0.030	0.008	3.44
Pb	15.9	25.0	17.9	14.9	21.1	23.9	22.9	19.0	18.9	19.5	21.9	19.7	21.9	25.4	20.88	20	1.04
Bi	0.23	0.41	0.28	0.24	0.38	0.40	0.35	0.29	0.31	0.32	0.35	0.32	0.36	0.41	0.34	0.127	2.64
Th	5.00	6.32	6.06	4.39	6.63	6.51	6.07	5.54	5.65	5.96	6.29	5.66	6.77	6.84	6.09	10.7	0.57
U	3.07	4.74	3.53	3.27	4.43	4.77	4.56	4.03	4.37	4.38	4.60	4.74	4.69	4.23	4.14	2.8	1.48

Av – the average value; UCC – the upper continental crust value; EF – the ratio of element content in oil shale to the upper continental crust.

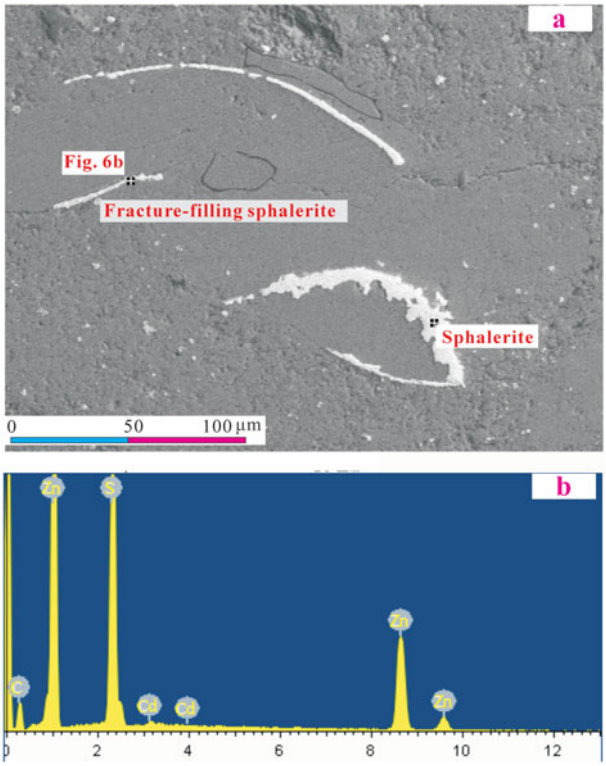

Figure 6 (Colour online) Sphalerite identified by SEM (back-scattered images) and EDX spectra in the Bilong Co. oil shale, sample 11NO.20-18.

enriched in the Bilong Co. oil shale, with enrichment factors (EF, the ratio of element content in the oil shale to the UCC) of 48.4, 30.0, 13.1, 6.53 and 4.15, respectively. Elements Li, F, V, Co, Cu, Cs, Hg and Bi have enrichment values > 1.52, while Be, Zr, Nb, Sn, Hf, Ta and W are depleted, with an EF less than 0.5. All other elements studied show more or less the same concentration as the UCC values, with an EF between 1.48 and 0.52.

The Bilong Co. oil shale samples are enriched in Li, Be, Sc, V, Co, Ni, Zn, Ga, Se, Rb, Zr, Nb, Mo, Cd, Sn, Cs, Ba, Hf, Ta, W, Hg, Pb, Bi, Th, U and rare earth elements (REEs) in comparison with the average for marine oil shale from China, as reported by Fu *et al.* (2015) (Table 3). Averages for F, As and Sr are lower, and those of Cr and Cu are close to the arithmetic means for the corresponding elements in Chinese marine oil shale samples (Fu *et al.* 2015).

5. Discussion

Seawater and stream water usually contain very low concentrations of trace elements. Thus, the water alone could not have accounted for the high concentrations of these elements observed in the Bilong Co. oil shale. Elevated concentrations of trace elements in the Bilong Co. oil shale are possibly related to input from volcanic ashes, groundwater, magmatic/hydrothermal fluids and the sediment-source rocks. Three processes were probably responsible for the geochemical anomalies found in the Bilong Co. oil shale: (1) the characteristics of the detrital materials from the sediment-source region, (2) marine influence during deposition, and (3) multi-stage hydrothermal activities.

5.a. Detrital materials from the sediment-source region

The modes of occurrence of quartz particles in the Bilong Co. oil shale (Fig. 4b), occurring mainly as fine particles forming a matrix, indicate that they were from detrital materials of terrigenous origin.

Clay minerals are common minerals in the Bilong Co. oil shale, and exhibit high concentrations in some oil shale samples (e.g. 11NO.20-2, 11NO.20-5, 11NO.20-15, 11NO.20-18, 11BL20-1 and 11BL20-3, Table 2). They occur mainly as irregular masses (Fig. 4a) as mentioned in Section 4.b above, and are probably of clastic origin.

Feldspars in sediments are mostly detrital minerals of terrigenous origin (e.g. Moore & Esmaeili, 2012; Dai *et al.* 2013). Feldspar apparently derived from epigenetic hydrothermal fluids, however, has been found in a number of coal deposits (Zhao *et al.* 2012), mostly associated with igneous activity. In the Qiangtang Basin, the igneous activity and emplacement ages are at about 205–220 Ma during early Mesozoic time (Fu *et al.* 2010), which are earlier than the age of the process of oil shale deposition (Early Jurassic). Additionally, feldspars occur mainly as disseminated grains identified by optical microscopy analyses, indicating a clastic origin.

The sediment-source region for the Bilong Co. oil shale is the central uplift, which is composed of the Late Triassic Nadi Kangri Formation volcanic-volcaniclastic rocks (Fu *et al.* 2012). The chemical compositions of the oil shale samples included in the present study further support this point of view. Al_2O_3/TiO_2 ratios have also been used to interpret the provenance of sedimentary rocks (e.g. Hayashi *et al.* 1997; He *et al.* 2010; Dai *et al.* 2013), because of the similar ratios of these effectively immobile elements in sedimentary rocks to those in their parent rocks (Hayashi *et al.* 1997). Typical Al_2O_3/TiO_2 ratios are from 3–8, 8–21 and 21–70 for sediments derived from mafic, intermediate and felsic igneous rocks, respectively (Hayashi *et al.* 1997). In the Bilong Co. oil shale, the Al_2O_3/TiO_2 ratios of the oil shale samples are from 23.8 to 30.5 (Table 4) indicating a mainly felsic source. Other ratios, such as La/Sc, Th/Sc, Cr/Th and $(La/Lu)_N$ are also significantly different in mafic and felsic source rocks and can, therefore, provide information about the provenance of sedimentary rocks (Armstrong-Altrin *et al.* 2004). The $(La/Lu)_N$, La/Sc, Th/Sc and Cr/Th ratios for the oil shale samples from the Bilong Co. oil shale are similar to those of the Nadi Kangri felsic volcanic source rocks (Table 4), consistent with input of detrital materials of terrigenous origin from those felsic volcanic rock materials.

REE distribution patterns have also been used as tracers to identify sources of oil shale sediments (Fu *et al.* 2011). The oil shale samples from the Bilong

https://doi.org/10.1017/S0016756815000758 Published online by Cambridge University Press

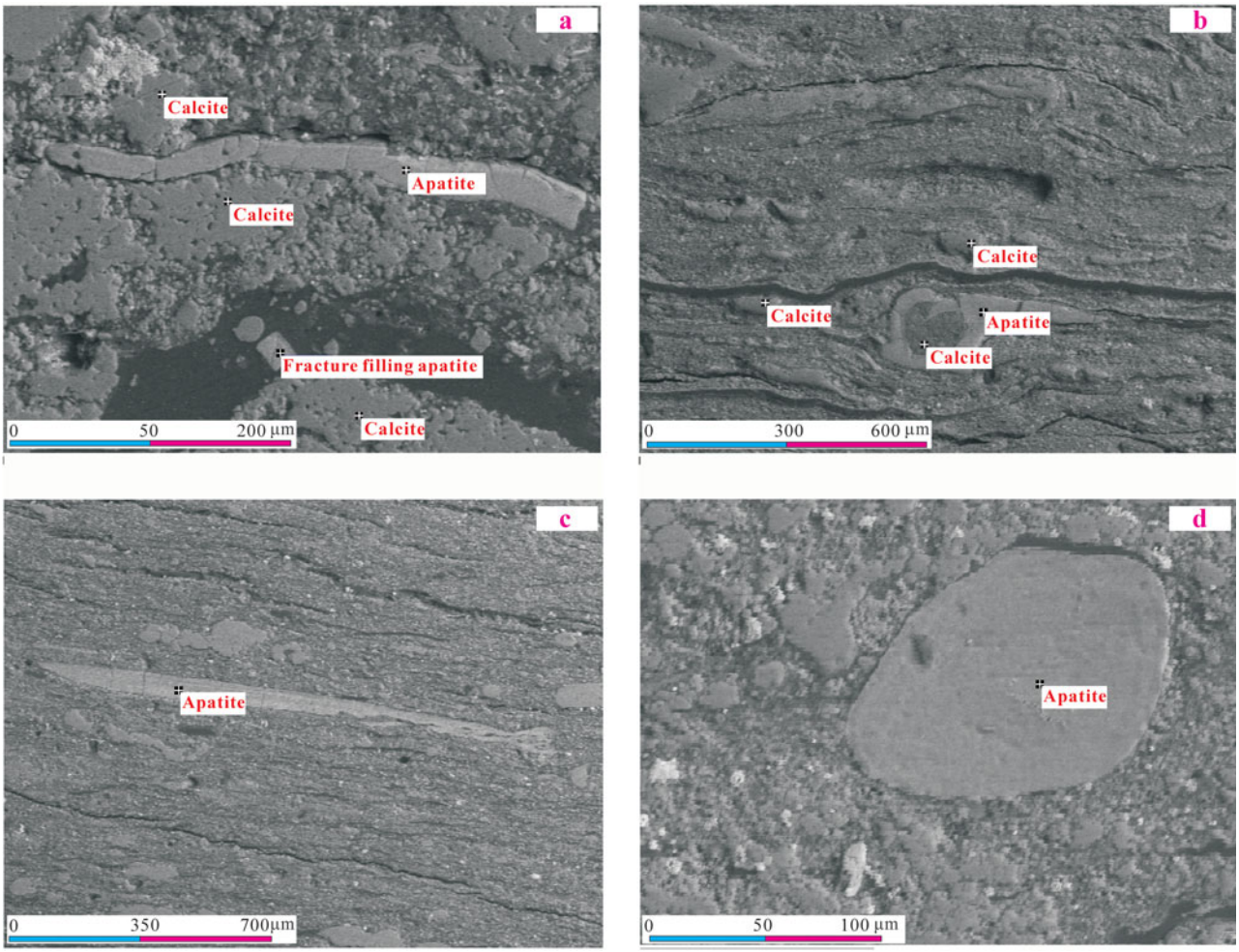

Figure 7. (Colour online) Apatite in oil shale samples from the Bilong Co oil shale. (a, b) Fracture-filling apatite, samples 11NO.20-13 and 11BL20-5; (c) banded apatite, sample 11NO.20-5; (d) disseminated-grain apatite, sample 11BL20-6 (SEM and back-scattered electron image).

Table 4. Range of elemental ratios of the oil shale samples from the Bilong Co. oil shale compared to the ratios in the Nadi Kangri Formation felsic rocks and UCC

Elemental ratio	Range of oil shale[a]	Range of the Nadi Kangri Formation felsic rocks[b]	Upper Continental Crust[c]
Al_2O_3/TiO_2	23.8–30.5(average 26.4)	12.7–98.0(average 36.1)	33.3
La/Sc	2.05–2.49(average 2.27)	1.62–4.22(average 2.72)	2.73
Th/Sc	0.71–0.87(average 0.80)	0.55–1.14(average 0.80)	0.97
Cr/Th	7.09–9.73(average 8.05)	0.63–9.67(average 3.76)	3.27
δEu	0.91–1.12(average 1.02)	0.83–1.52(average 1.14)	1.00
$(La/Yb)_N$	0.80–1.14(average 1.04)	0.56–1.12(average 0.89)	1.00

a – this study; b – Fu *et al*. (2010), Wang *et al*. (2008); c – Taylor & McLennan (1995).

Co. area have slightly positive or negligible Eu anomalies (average δEu = 1.02), which is typical for the REE characteristics of the felsic volcanic rocks in the Nadi Kangri Formation (Table 4). The REE distribution patterns in the Nadi Kangri felsic volcanic rocks are similar to those in the oil shale samples (Fig. 9), indicating that the REEs in the Bilong Co. oil shale were probably derived from the Nadi Kangri felsic volcanic rock materials. Input of sediments from these sources may have led to the enrichment of trace elements Li, Cr and Cs in the oil shale. However, the enrichment factor is low with the EF between 1.40 and 1.82 (Table 3).

Elevated concentrations of trace elements in the Bilong Co. oil shale are also possibly related to weathering. The chemical index of alteration (CIA) is a method of quantifying the degree of source weathering (Nesbitt & Young, 1982). CIA was defined as $(Al_2O_3/(Al_2O_3 + CaO^* + Na_2O + K_2O)) \times 100$ following Nesbitt & Young (1982, 1989), Fedo, Nesbitt & Young (1995) and Fedo, Eriksson & Krogstad (1996). The oxides are expressed as molar proportions. The molar CaO is corrected for the presence of carbonate and apatite as for the CIA (Fedo, Nesbitt & Young, 1995) to consider only the silicate-bound Ca (CaO^*).

https://doi.org/10.1017/S0016756815000758 Published online by Cambridge University Press

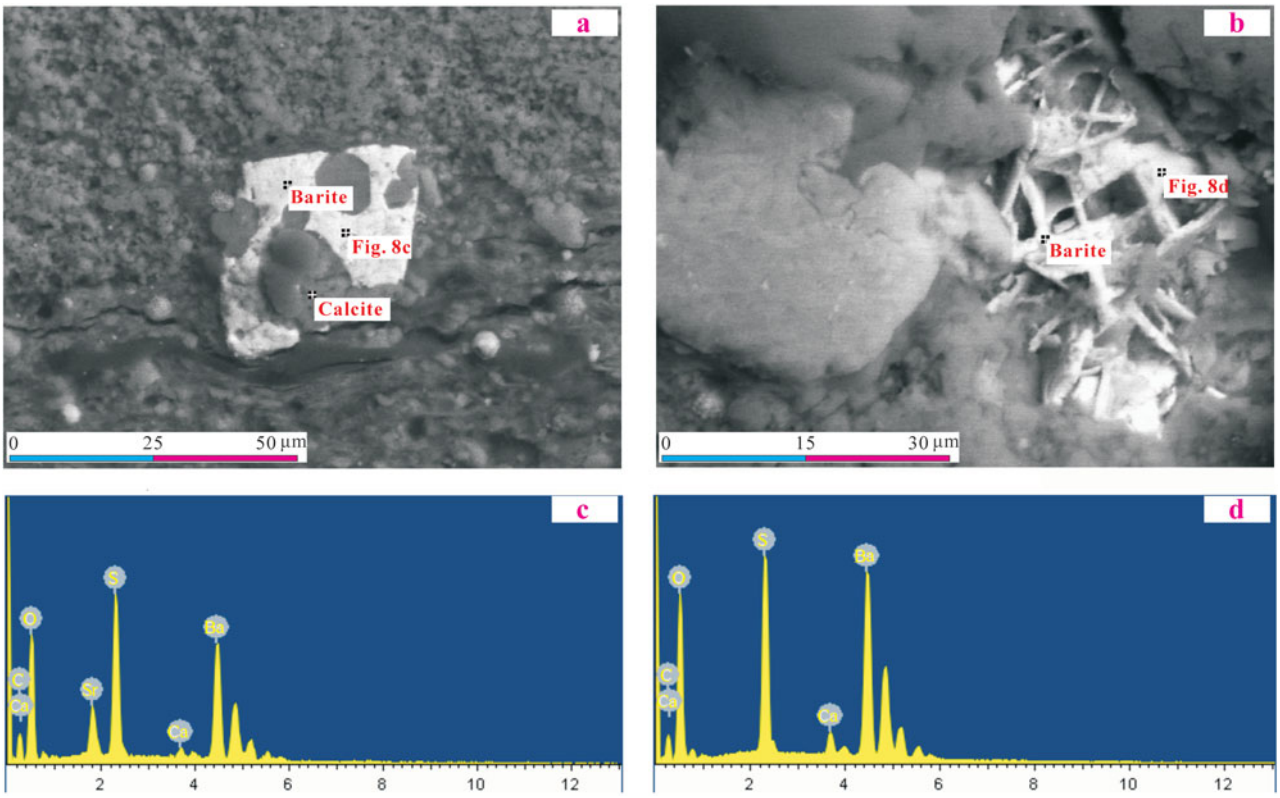

Figure 8. (Colour online) Barite identified by SEM (back-scattered images) and EDX spectra in oil shale samples from the Bilong Co. oil shale, samples 11NO.20-12 and 11BL20-8.

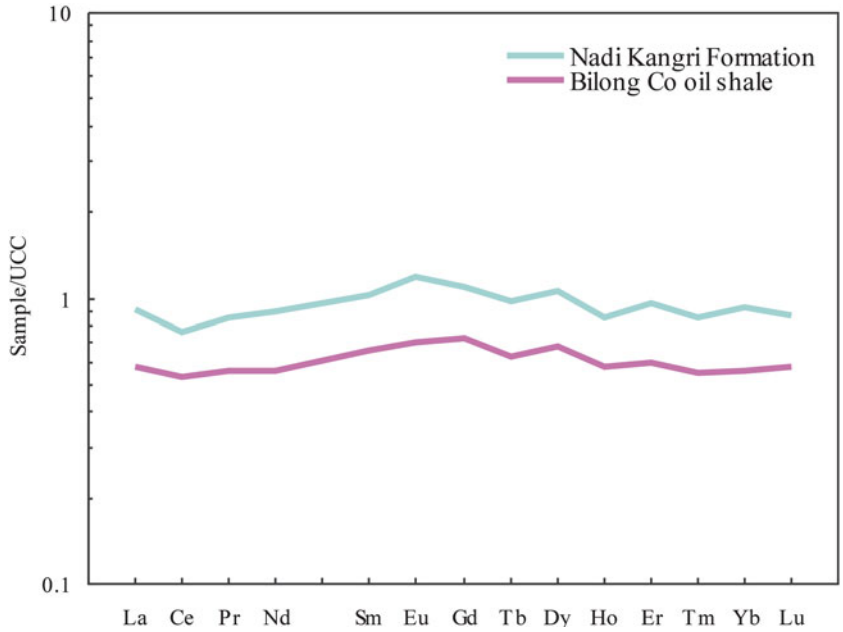

Figure 9. (Colour online) Distribution patterns of rare earth elements in oil shale samples from the Bilong Co. oil shale. Note the similarity in REE patterns for oil shale samples and the Nadi Kangri felsic volcanic rocks.

In the present study, the CIA values of the oil shale samples range from 71 to 79, with an average of 76 (Table 1). These values indicate a moderate degree of chemical weathering of the source area. The elements of the alkaline earth group are the most mobile during continental weathering (Nesbitt, Markovics & Price, 1980). A weakly positive correlation between CIA and alkaline earth group elements (Fig. 10) indicates a slight or negligible influence of weathering.

5.b. Marine influence during the oil shale deposition

The Bilong Co. oil shale was deposited in lagoonal environments (Fu *et al*. 2014), and thus the influence of

https://doi.org/10.1017/S0016756815000758 Published online by Cambridge University Press

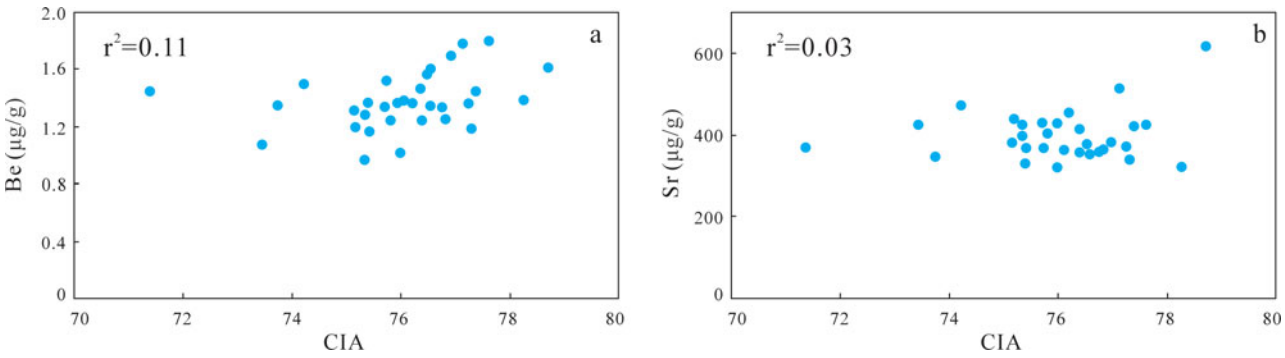

Figure 10. (Colour online) Relationship between CIA and alkaline earth elements (a) Be and (b) Sr.

marine conditions on the geochemical characteristics of the oil shale samples appears to have been significant. As mentioned in Section 4.b above, calcite and dolomite occur mainly as grains (Figs 3a, b), indicating an authigenic origin from seawater. Therefore, the high concentrations of Ca and Mg in the Bilong Co. oil shale were probably derived from seawater. The nodular and framboidal occurrences of pyrite (Figs 4b, 5) indicate that the minerals with such modes of occurrence were of syngenetic or early diagenetic origin. The Fe in these minerals was probably derived from seawater.

The Bilong Co. oil shale was deposited in anoxic conditions (Fu *et al*. 2014). This point of view is supported by the high concentration of redox-sensitive trace elements (e.g. V, Co, Ni, Cu, Mo and U), which are higher in anoxic marine facies than in deposits formed under oxic marine conditions (Hetzel *et al*. 2011). In such a setting, these trace elements were probably taken up by authigenic mineral phases and/or organic matter (Algeo & Maynard, 2004). The TFeO (TFeO = $FeO + 0.9 \times Fe_2O_3$) values can be correlated very well with the V (Fig. 11a), Co (Fig. 11b), Ni (Fig. 11c) and Cu (Fig. 11d) concentrations in the studied oil shales, and exhibit moderate positive correlations with U (Fig. 11e), suggesting that these trace elements may be related to the Fe-sulfides (pyrite). Additionally, As, Se and Bi may also occur as Fe-sulfides (pyrite) in the Bilong Co. oil shale as evidenced by the positive relationships between TFeO and the As (Fig. 11f), Se (Fig. 11g) and Bi (Fig. 11h) contents. Previous studies have shown that Mo has high concentrations in oil shale seams of this deposit compared with the adjacent roof and floor strata (Fu *et al*. 2014). The enrichment of Mo may thus be attributed to its links with pyrite and sulfur-rich organic matter (Tribovillard *et al*. 2004).

The high Sr content of the oil shale also seems to indicate the influence of seawater on the oil shale, because Sr is deposited directly from seawater (Reimann & de Caritat, 1998). The high ratio of Sr/Ba (average 1.48) in the Bilong Co. oil shale further supports the above observations.

5.c. Hydrothermal fluid influence

Hydrothermal fluid is another important factor that may be responsible for the trace-element and mineral characteristics of the Bilong Co. oil shale. This is supported by mineralogical and geochemical evidence.

As mentioned in Section 4.b above, barite was identified in some oil shale samples. Barite can precipitate in a variety of settings, such as marine, hydrothermal, cold seep and diagenetic environments (Paytan *et al*. 2002). The various environments of formation result in a range of saturation conditions and precipitation rates, thus resulting in differences in crystal sizes and morphologies of barite (Griffith & Paytan, 2012). In the Bilong Co. oil shale, the relationships between barite and calcite (Fig. 8a) indicate that barite was formed later than the associated calcite. The barite contains trace amounts of Ca (Figs 8c, d), which further supports the above observations. The Ca was probably leached from the nearby limestones by hydrothermal fluids.

Sphalerite was also detected by SEM-EDX analysis in the Bilong Co. oil shale, and occurs mainly as shell replacements (Fig. 6a), suggesting an epigenetic hydrothermal origin. Deposition of sphalerite may take place over wide temperature ranges including low-, medium- and high-temperature hydrothermal stages, and its chemical composition is a function of the formation temperature (Ramdohr, 1980). Low-temperature sphalerite commonly has a low Fe content with relatively high concentrations of Cd (Ye *et al*. 2011). The sphalerite from the Bilong Co. oil shale is depleted in Fe and has relatively high concentrations of Cd, indicating a low-temperature hydrothermal origin.

Fracture-filling pyrite (Figs 5e,f) and shell-replacement pyrite (Figs 5d) were also found in some of the oil shale samples as discussed in Section 4.b above. The relationships between pyrite and calcite (Fig. 5f) indicate that the pyrite was formed later than the associated calcite. The pyrite contains trace amounts of Ca (Figs 5g, h), which supports a hydrothermal origin. Calcium was also probably leached from the nearby limestones by hydrothermal fluids (Dai *et al*. 2013).

https://doi.org/10.1017/S0016756815000758 Published online by Cambridge University Press

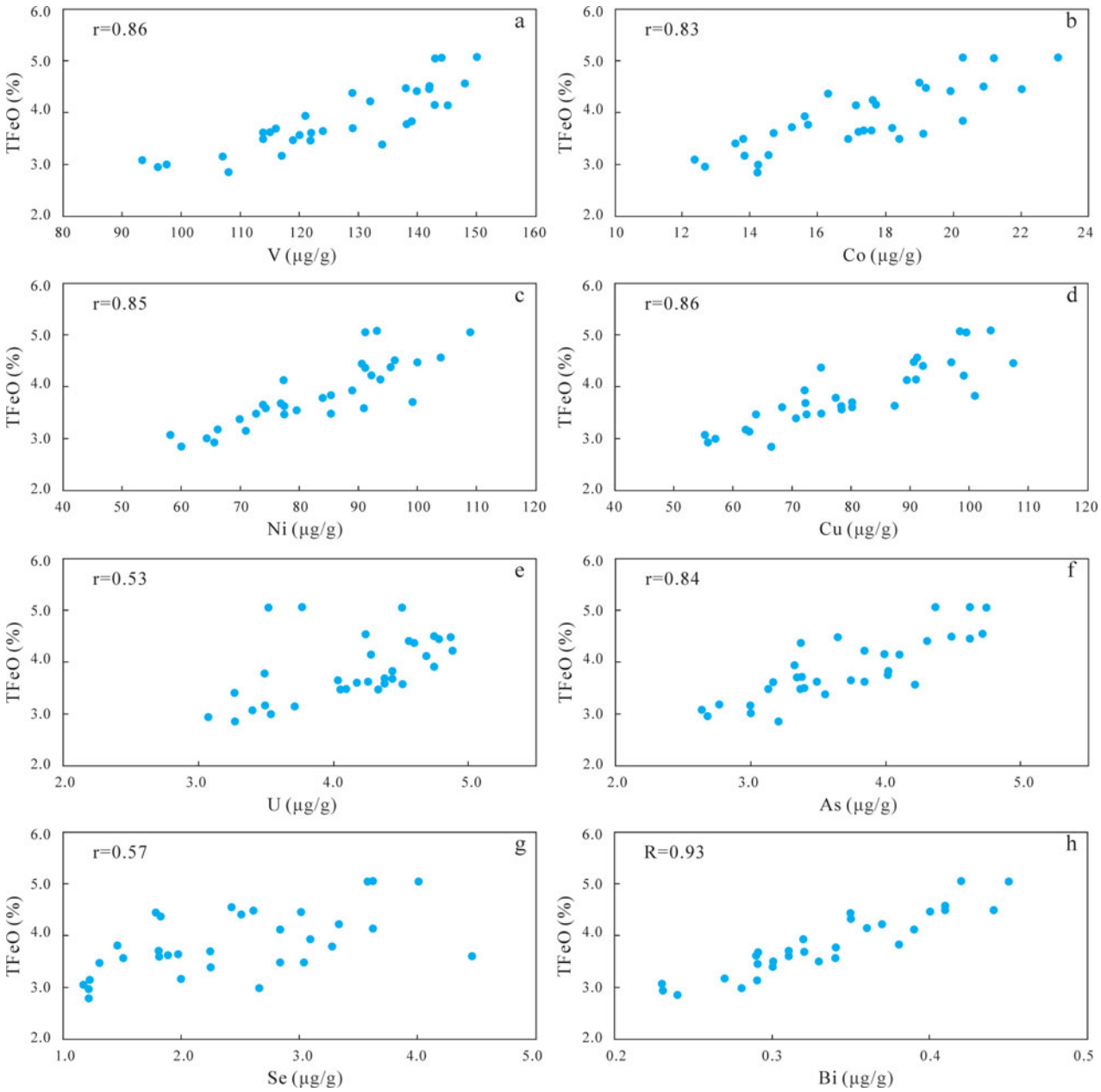

Figure 11. (Colour online) Relationship between TFeO and trace elements (a) V, (b) Co, (c) Ni, (d) Cu, (e) U, (f) As, (g) Se and (h) Bi.

The geochemical evidence for the hydrothermal activities is the enrichment of Cd in the oil shale samples. A significantly positive correlation between Cd and Zn (Fig. 12) indicates that Cd is associated mainly with Zn-bearing minerals. The sphalerite is the main carrier of Cd identified by SEM-EDX analysis (Fig. 6b). These data suggest that Cd was derived from hydrothermal fluids.

In addition to high Cd of hydrothermal fluid origin, the high concentration of F in the Bilong Co. oil shale was also derived from hydrothermal fluids. The apatite is the main carrier of F. The relationships between calcite and apatite (Fig. 7b) suggest that apatite was formed later than the associated calcite. The calcite is of authigenic origin as mentioned in Section 5.b above, but the apatite is of epigenetic hydrothermal origin. Fracture-filling occurrences of apatite (Fig. 7a) were also identified by SEM-EDX analysis, which is thought to have been derived from hydrothermal solutions. These data suggest that F has hydrothermal

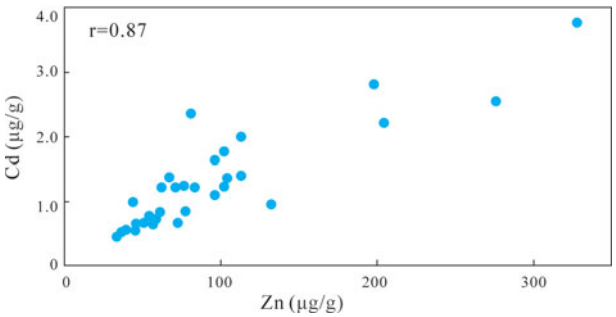

Figure 12. (Colour online) Concentration of Cd v. Zn, showing a significantly positive correlation.

https://doi.org/10.1017/S0016756815000758 Published online by Cambridge University Press

sources, although banded (Fig. 7c) and disseminated grains (Fig. 7d) in a small proportion of the apatite may indicate a seawater origin.

6. Conclusions

(1) The minerals identified in the Bilong Co. oil shale include calcite, quartz, illite, feldspar and dolomite, and trace amounts of siderite, magnesite, halite, haematite, zeolite, amphibole, gypsum, anhydrite, apatite, pyrite, sphalerite, barite and mixed-layer illite/smectite. The clay minerals, quartz and feldspar are detrital materials of terrigenous origin; the carbonate minerals and nodular- and framboidal-pyrite were authigenic or biogenic deposits from seawater; and barite, sphalerite and fracture-filling pyrite were derived from hydrothermal solutions.

(2) The most enriched trace elements in the Bilong Co. oil shale relative to the UCC are Se (48.4×), Mo (30.0×), Cd (13.1×), As (6.53×) and Ni (4.15×); Li, F, V, Co, Cu, Cs, Hg and Bi also have high concentrations, with enrichment factors from 1.52 to 3.44, compared to UCC values. The Bilong Co. oil shales are richer in many trace elements, including Li, Be, Sc, V, Co, Ni, Zn, Ga, Se, Rb, Zr, Nb, Mo, Cd, Sn, Cs, Ba, Hf, Ta, W, Hg, Pb, Bi, Th, U and REEs, in comparison to averages for marine oil shale in China.

(3) Elements thought to be of terrigenous origin in the Bilong Co. oil shale appear to have originated from the Nadi Kangri felsic volcanic rocks. Input of sediments from this source may have also led to the enrichment of trace elements Li, Cr and Cs in the oil shale. However, if so, the enrichment factor is low.

(4) It seems that seawater and hydrothermal activities influenced the geological compositions of the Bilong Co. oil shale. The enrichment of V, Co, Ni, Cu, Mo, As, Se, Bi and U in the oil shale samples was due to marine influence, while F, Zn and Cd were mainly derived from hydrothermal fluids.

Acknowledgements. This work was supported by the National Natural Science Foundation of China (Nos. 41172098 and 40972087), the Sichuan Youth Science & Technology Foundation (No. 09ZQ026-006) and the Chinese National Oil and Gas Special Project (No.XQ-2009-01). We thank two unknown reviewers for their constructive comments on the manuscript.

References

ALGEO, T. J. & MAYNARD, J. B. 2004. Trace-element behavior and redox facies in core shales of Upper Pennsylvanian Kansas-type cyclothems. *Chemical Geology* **206**, 289–318.

ARMSTRONG-ALTRIN, J. S., LEE, Y. I., VERMA, S. P. & RAMASAMY, S. 2004. Geochemistry of sandstones from the Upper Miocene Kudankulam Formation, southern India: implication for provenance, weathering and tectonic setting. *Journal of Sedimentary Research* **74**, 285–97.

BARUAH, M. K., KOTOKY, P., BARUAH, J. & BORA, G. C. 2005. Extent of lead in high sulphur Assam coals. *Fuel Processing Technology* **86**, 731–4.

BENCKO, V. & SYMON, K. 1977. Health aspects of burning coal with a high arsenic content: 1. Arsenic in hair, urine, and blood in children residing in a polluted area. *Environmental Research* **13**, 378–85.

CHEN, L., YI, H. S., HU, R. Z., ZHONG, H. & ZOU, Y. R. 2005. Organic geochemistry of the early Jurassic oil shale from the Shuanghu area in northern Tibet and the early Toarcian oceanic anoxic event. *Acta Geologica Sinica – English Edition* **79**, 392–7.

DAI, S. F., REN, D. Y., CHOU, C.-L., FINKELMAN, R. B., SEREDIN, V. V. & ZHOU, Y. P. 2012. Geochemistry of trace elements in Chinese coals: a review of abundances, genetic types, impacts on human health, and industrial utilization. *International Journal of Coal Geology* **94**, 3–21.

DAI, S. F., REN, D. Y., TANG, Y. G., YUE, M. & HAO, L. M. 2005. Concentration and distribution of elements in Late Permian coals from western Guizhou Province, China. *International Journal of Coal Geology* **61**, 119–37.

DAI, S. F., TIAN, L. W., CHOU, C.-L., ZHOU, Y. P., ZHANG, M. Q., ZHAO, L., WANG, J. M., YANG, Z., CAO, H. Z. & REN, D. Y. 2008. Mineralogical and compositional characteristics of Late Permian coals from an area of high lung cancer rate in Xuan Wei, Yunnan, China: occurrence and origin of quartz and chamosite. *International Journal of Coal Geology* **76**, 318–27.

DAI, S. F., ZHANG, W. G., SEREDIN, V. V., WARD, C. R., HOWER, J. C., SONG, W. J., WANG, X. B., LI, X., ZHAO, L. X., KANG, H., ZHENG, L. C., WANG, P. P. & ZHOU, D. 2013. Factors controlling geochemical and mineralogical compositions of coals preserved within marine carbonate successions: a case study from the Heshan Coalfield, southern China. *International Journal of Coal Geology* **109–110**, 77–100.

DING, W. L., WAN, H., SU, A. G. & HE, Z. H. 2011. Characteristics of Triassic marine source rocks and prediction of favorable source kitchens in Qiangtang Basin, Tibet. *Energy Exploration & Exploitation* **29**, 143–60.

DZG 20.10-1990. 1990. *Geology Mineral Industry Standard of P.R. China: Rock and Mineral Analysis* (in Chinese).

DZ/T 0223-2001. 2001. *Geology Mineral Industry Standard of P.R. China: The General Analysis Rules for Inductively Coupled Plasma Mass Spectrometry* (in Chinese).

FEDO, C. M., ERIKSSON, K. A. & KROGSTAD, E. J. 1996. Geochemistry of shales from the (~3.0 Ga) Buhwa Greenstone Belt, Zimbabwe: implications for provenance and source-area weathering. *Geochimica et Cosmochimica Acta* **60**, 1751–63.

FEDO, C. M., NESBITT, H. W. & YOUNG, G. M. 1995. Unravelling the effects of potassium metasomatism in sedimentary rocks and paleosols, with implications for paleoweathering conditions and provenance. *Geology* **23**, 921–4.

FINKELMAN, R. B., BELKIN, H. E. & ZHENG, B. S. 1999. Health impacts of domestic coal use in China. *Proceedings of the National Academy of Sciences of the United States of America* **96**, 3427–31.

FU, X. G., LIAO, Z. L., WANG, J. & CHEN, W. B. 2008. Geochemistry and significance of oil seepages in the Zaring area of the southern Qiangtang depression, northern Tibet. *Acta Sedimentologica Sinica* **26**, 697–704 (in Chinese with English abstract).

FU, X. G., TAN, F. W., FENG, X. L., WANG, D., CHEN, W. B., SONG, C. Y. & ZENG, S. Q. 2014. Early Jurassic

https://doi.org/10.1017/S0016756815000758 Published online by Cambridge University Press

anoxic conditions and organic accumulation in the eastern Tethys. *International Geology Review* **56**, 1450–65.

Fu, X. G., Wang, J., Tan, F. W., Chen, M. & Chen, W. B. 2010. The Late Triassic rift-related volcanic rocks from eastern Qiangtang, northern Tibet (China): age and tectonic implications. *Gondwana Research* **17**, 135–44.

Fu, X. G., Wang, J., Tan, F. W., Feng, X. L. & Zeng, S. Q. 2013. Minerals and potentially hazardous trace elements in the Late Triassic coals from the Qiangtang Basin, China. *International Journal of Coal Geology* **116–117**, 93–105.

Fu, X. G., Wang, J., Tan, F. W., Feng, X. L., Zeng, S. Q., Chen, W. B. & Wang, D. 2015. Minerals and potentially hazardous trace elements in marine oil shale: new insights from the Shengli River North surface mine, northern Tibet, China. *Environmental Earth Sciences* **104**, 495–511.

Fu, X. G., Wang, J., Tan, F. W. & Zeng, Y. H. 2009. Sedimentological investigations of the Shengli River-Changshe Mountain oil shale (China): relationships with oil shale formation. *Oil Shale* **26**, 373–81.

Fu, X. G., Wang, J., Zeng, Y. H., Tan, F. W. & Feng, X. L. 2011. Concentration and mode of occurrence of trace elements in marine oil shale from the Bilong Co area, northern Tibet, China. *International Journal of Coal Geology* **85**, 112–22.

Fu, X. G., Wang, J., Zeng, Y. H., Tan, F. W. & Feng, X. L. 2012. Source regions and the sedimentary paleoenvironment of marine oil shale from the Bilong Co area, northern Tibet, China: an Sr-Nd isotopic study. *Oil Shale* **29**, 306–21.

Griffith, E. M. & Paytan, A. 2012. Barite in the ocean – occurrence, geochemistry and palaeoceanographic applications. *Sedimentology* **59**, 1817–35.

Hayashi, K. I., Fujisawa, H., Holland, H. D. & Ohmoto, H. 1997. Geochemistry of ~1.9 Ga sedimentary rocks from northeastern Labrador, Canada. *Geochimimica et Cosmochimica Acta* **61**, 4115–37.

He, B., Xu, Y.-G., Zhong, Y.-T. & Guan, J-P. 2010. The Guadalupian–Lopingian boundary mudstones at Chaotian (SW China) are clastic rocks rather than acidic tuffs: implication for a temporal coincidence between the end-Guadalupian mass extinction and the Emeishan volcanism. *Lithos* **119**, 10–9.

Hetzel, A., März, C., Vogt, C. & Brumsack, H.-J. 2011. Geochemical environment of Cenomanian – Turonian black shale deposition at Wunstorf (northern Germany). *Cretaceous Research* **32**, 480–94.

Hillier. 2000. Accurate quantitative analysis of clay and other minerals in sandstones by XRD: comparison of a Rietveld and a reference intensity ratio (RIR) method and the importance of sample preparation. *Clay Minerals* **35**, 291–302.

Liu, Z. J., Yang, H. L., Dong, Q. S., Zhu, J. W., Guo, W., Ye, S. Q., Liu, R., Meng, Q. T., Zhang, H. L. & Gan, S. C. 2009. *Oil Shale in China*, pp. 1157–67. Beijing: Petroleum Industry Press (in Chinese with English abstract).

Moore, F. & Esmaeili, A. 2012. Mineralogy and geochemistry of the coals from the Karmozd and Kiasar coal mines, Mazandaran province, Iran. *International Journal of Coal Geology* **96–97**, 9–21.

Nesbitt, H. W., Markovics, G. & Price, R. C. 1980. Chemical processes affecting alkalis and alkaline earths during continental weathering. *Geochimica et Cosmochimica Acta* **44**, 1659–66.

Nesbitt, H. W. & Young, G. M. 1982. Early Proterozoic climates and plate motions inferred from major element chemistry of lutites. *Nature* **299**, 715–7.

Nesbitt, H. W. & Young, G. M. 1989. Formation and diagenesis of weathering profiles. *Journal of Geology* **97**, 129–47.

Otto, C. S. 1997. Mesozoic–Cenozoic history of deformation and petroleum systems in sedimentary basins of Central Asia; implications of collisions on the Eurasian margin. *Petroleum Geoscience* **3**, 327–41.

Pattan, J. N. & Pearce, N. J. G. 2009. Bottom water oxygenation history in southeastern Arabian Sea during the past 140 ka: results from redox-sensitive elements. *Palaeogeography, Palaeoclimatology, Palaeoecology* **280**, 396–405.

Paytan, A., Mearon, S., Cobb, K. & Kastner, M. 2002. Origin of marine barite deposits: Sr and S isotope characterization. *Geology* **30**, 747–50.

Ramdohr, P. 1980. *The Ore Minerals and their Intergrowths*, pp. 1–1205. Oxford: Pergamon Press.

Reimann, C. & de Caritat, P. 1998. *Chemical Elements in the Environment*. Berlin: Springer, 397 pp.

Seredin, V. V. & Dai, S. F. 2012. Coal deposits as potential alternative sources for lanthanides and yttrium. *International Journal of Coal Geology* **94**, 67–93.

Seredin, V. V. & Finkelman, R. B. 2008. Metalliferous coals: a review of the main genetic and geochemical types. *International Journal of Coal Geology* **76**, 253–89.

SY/T 6210-1996. 1996. *Oil and Gas Standard of P.R. China: X-ray diffraction quantitative analysis methods of the clay minerals and common non-clay minerals in sedimentary rocks* (in Chinese).

Taylor, S. R. & Mclennan, S. M. 1995. The geochemical evolution of the continental crust. *Reviews of Geophysics* **33**, 241–65.

Tribovillard, N., Algeo, T. J., Lyons, T. & Riboulleau, A. 2006. Trace metals as paleoredox and paleoproductivity proxies: an update. *Chemical Geology* **232**, 12–32.

Tribovillard, N., Riboulleau, A., Lyons, T. & Baudin, F. 2004. Enhanced trapping of molybdenum by sulfurized marine organic matter of marine origin in Mesozoic limestones and shales. *Chemical Geology* **213**, 385–401.

Wang, J., Tan, F. W., Li, Y. L., Li, Y. T., Chen, M., Wang, C. S., Guo, Z. J., Wang, X. L., Du, B. W. & Zhu, Z. F. 2004. *The Potential of the Oil and Gas Resources in Major Sedimentary Basins on the Qinghai–Xizang Plateau*, pp. 34–38. Beijing: Geological Publishing House (in Chinese with English abstract).

Wang, C. S. & Zhang, S. M. 1987. The discovery of oil shales in the Shuanghu area, northern Tibet, China. *Geology in China* **8**, 29–31 (in Chinese).

Wei, H. Y., Chen, D. Z., Wang, J. G., Yu, H. & Tucher, M. E. 2012. Organic accumulation in the lower Chihsia Formation (Middle Permian) of South China: constraints from pyrite morphology and multiple geochemical proxies. *Palaeogeography, Palaeoclimatology, Palaeoecology* **353–355**, 73–86.

Westermann, S., Stein, M., Matera, V., Fiet, N., Fleitmann, D., Adatte, T. & Föllmi, K. B. 2013. Rapid changes in the redox conditions of the western Tethys Ocean during the early Aptian oceanic anoxic event. *Geochimica et Cosmochimica Acta* **121**, 467–86.

Ye, L., Cook, N. J., Ciobanu, C. L., Liu, Y. P., Zhang, Q., Liu, T. G., Gao, W., Yang, Y. L. & Danyushevskiy, L. 2011. Trace and minor elements in sphalerite from

https://doi.org/10.1017/S0016756815000758 Published online by Cambridge University Press

base metal deposits in South China: a LA-ICPMS study. *Ore Geology Reviews* **39**, 188–217.

YEOMANS, J. C. & BREMNER, J. M. 1988. A rapid and precise method for routine determination of organic carbon in soil. *Communication in Soil Science and Plant Analysis* **19**, 1467–76.

YI, H. S., CHEN, L., JENKYNS, H., DA, X. J., XIA, M. Q., XU, G. W. & JI, C. J. 2013. The Early Jurassic oil shales in the Qiangtang Basin, northern Tibet: biomarkers and Toarcian oceanic anoxic events. *Oil Shale* **30**, 441–55.

ZHAO, L., WARD, C. R., FRENCH, D. & GRAHAM, I. T. 2012. Mineralogy of the volcanic-influenced Great Northern coal seam in the Sydney Basin, Australia. *International Journal of Coal Geology* **94**, 94–110.

ZHAO, Y. C., ZHANG, J. Y., HUANG, W. C., WANG, Z. H., LI, Y., SONG, D. Y., ZHAO, F. H. & ZHENG, C. G. 2008. Arsenic emission during combustion of high arsenic coals from Southwestern Guizhou, China. *Energy Conversion and Management* **49**, 615–24.

https://doi.org/10.1017/S0016756815000758 Published online by Cambridge University Press